Available online at www.sciencedirect.com
ScienceDirect
Icarus 187 (2007) 167–176
ICARUS
www.elsevier.com/locate/icarus

The United Kingdom Infrared Telescope Deep Impact observations: Light curve, ejecta expansion rates and water spectral features

Robert J. Barber [a], Steve Miller [a,*], Tom Stallard [a] Jonathan Tennyson [a], Paul Hirst [b], Tim Carroll [b], Andy Adamson [b]

[a] *Department of Physics and Astronomy, University College London, London WC1E 6BT, UK*
[b] *Joint Astronomy Centre, 660 N. A'ohoku Place, University Park, Hilo, HI 96720, USA*

Received 12 April 2006; revised 31 July 2006

Available online 24 October 2006

Abstract

We present results from the United Kingdom Infrared Telescope observations of the impact of Deep Impact with Comet 9P/Tempel 1, on July 4, 2005 UT. These observations were carried out in conjunction with the worldwide observing campaign co-ordinated by K.J. Meech [Meech, K.J., and 208 colleagues, 2005. Science 310, 265–269]. The UKIRT team was the first to observe and announce the successful impact. At 05:50:52 (±2.5 s) UT the visible camera that is used to guide the telescope on the comet showed the start of a rapid rise in intensity, such that the visible brightness of Tempel 1 approximately doubled in 70 s. After that time there was a steady increase in the visible flux from the comet until it reached a maximum around 35 min post-impact, at which point it was more than ten times its original intensity. From an average of the time to maximum brightness and the time to noticeable intensity decline, we deduce that the material ejected by the impact expanded with a range of velocities between ∼125 and ∼390 m/s. We also observed water emission lines in the spectral region from 2.8945 to 2.8985 μm. We noted several water lines, which are known to be pumped by sunlight. But there was a lower intensity spectral component, which we propose may result from solar heating of icy grains freshly exposed by the impact.

Keywords: Comets; Infrared observations

1. Introduction

On July 4, 2005, NASA's Deep Impact (DI) mission delivered an impact of 19 gigajoules (gJ) to Comet 9P/Tempel 1. Full details of the impact itself have been given by A'Hearn et al. (2005), and will not be repeated here. Comets are of interest, intrinsically and because they preserve a record of chemical conditions in the early Solar System. The purpose of the mission was to excavate the surface of the comet, which had been processed considerably by sunlight, in order to reveal more pristine material. To complement the impact, there was a worldwide campaign using ground-based and orbiting observatories to record the effects of the impact in various wavelength regions. This campaign was co-ordinated by K. Meech, and initial results have been published (Meech et al., 2005). Among the most important of the results published are images of the dust coma produced by the impact, the identification of spectral lines from freshly released gases, and the comet's photometric behaviour. Light curves show that the comet's spatially integrated brightness increased by roughly an order of magnitude, from Magnitude 17 in the standard (Cousins) *R* band. Of particular interest, for our work, is the study by Mumma et al. (2005), which made use of high-resolution infrared spectra to identify species released by the impact. Most prominent among these was water, but they also identified methane, methanol, carbon monoxide, hydrogen cyanide, acetylene, ethane and formaldehyde.

The United Kingdom Infrared Telescope (UKIRT) on Mauna Kea, Hawaii, was the first observatory to report the success of DI (P. Hirst et al., telecom communication to the Deep Impact collaboration, 2005-07-04, 05:53 UT). The UKIRT observing team were making use of the facility high-resolution spec-

* Corresponding author. Fax: +44 (0) 20 7679 7145.
E-mail address: s.miller@ucl.ac.uk (S. Miller).

0019-1035/$ – see front matter
doi:10.1016/j.icarus.2006.08.017

trometer, CGS4, in echelle mode ($\lambda/\Delta\lambda \sim 18{,}500$) to observe emission features due to water. We also made use of the guider camera, which operates in the red end of the optical spectrum to follow the comet's brightness. Here we present the UKIRT light curve and a detailed analysis of its features. We also present an analysis of the spectral region observed, showing that it consists of two simultaneously evolving water components. Mumma et al.'s (2005) work gives us an invaluable point of departure for estimating water column densities and production rates.

2. The UKIRT *R* light curve

Our observations spanned the period from 2005, July 3–5 UT. In this paper we focus on the period from 2005, July 4 05:40–08:40 UT. The UKIRT visible guider CCD camera is normally used to guide the telescope on the object of interest: on July 4, 2005 UT it was being used in this mode. It has a variable sampling rate, and was being run at 20 Hz (one image per 0.05 s) on the Deep Impact Night. Thus UKIRT had the most sensitive instrument available in terms of time resolution to follow the events leading up to, during and subsequent to impact. At 05:50:52 UT the visible camera that is used to guide the telescope on the comet showed the start of a rapid rise in intensity, such that the visible brightness of Tempel 1 approximately doubled in 70 s. We now look at the light curve in some detail, since it holds clues to the processes occurring during cratering.

Fig. 1 shows the screen capture of the guider camera display, which includes the first portion of the raw light curve, time stamped by the Global Positioning System clock, which is used for telescope guidance, at July 3, 2005, 20:03:15 Hawaii Standard Time (HST), equivalent to July 4, 2005, 06:03:15 UT. (Note that the guider camera's trace is not stored electronically, and this paper perforce makes use of screen capture images of the visible intensity, with intensity shown as counts in the image.) The figure shows minutes prior to the stamped time as $-t$ min. The dark line shows the sky-subtracted intensity of the comet in a square of four (2×2) camera $0.9'' \times 0.9''$ pixels, with a total coverage on the sky of a $1.8'' \times 1.8''$ square. This corresponds to 1170×1170 km around Tempel 1. Thus the diagonal distance from the centre of the guider camera's "target box" to the corners is 827 km. The thinner, lighter trace shows the intensity of the sky in the surrounding twelve $0.9'' \times 0.9''$ pixels around the target box. It is this intensity that is used for sky subtraction—a feature that has a bearing on the later evolution of the target box light curve itself. The sharp decline in this trace shows that the impact occurred during Hawaiian twilight. (NB the sharp decrease in guidebox intensity every ~6 min is due "beam-switching".)

The target box (dark) trace shows that at some time between $t = -12$ and $t = -10$ min, the visible intensity of the comet began to increase rapidly. This two-minute region is shown in more detail in Fig. 2. The guider software automatically bins its 20-Hz measurements into blocks of ~1.9 s. There is a step-wise increase in intensity at $t =$ UT 06:03:15—11 m 09.5 s, ±2.5 s, after which time all of the measured intensities are greater than the comet's Pre-Impact Brightness (PIB). We take this stringent criterion as evidence of impact having occurred. This gives the UKIRT Impact Time at UT 05:52:05.5 ± 2.5 s, and is marked in Fig. 2. Henceforth times are presented relative to this time. This is outside of the range for impact time given by A'Hearn et al. (2005), which is based on the measurement of a "flash" at UT 05:52:01.5–UT 05:52:02.3. This time is also marked in Fig. 2. [That said, an interpretation of our data less stringent than our insistence that *all* intensities are greater than PIB could have our light curve increasing "monotonically" from the A'Hearn et al. (2005) Impact Time.] Meech et al. (2005) report that no

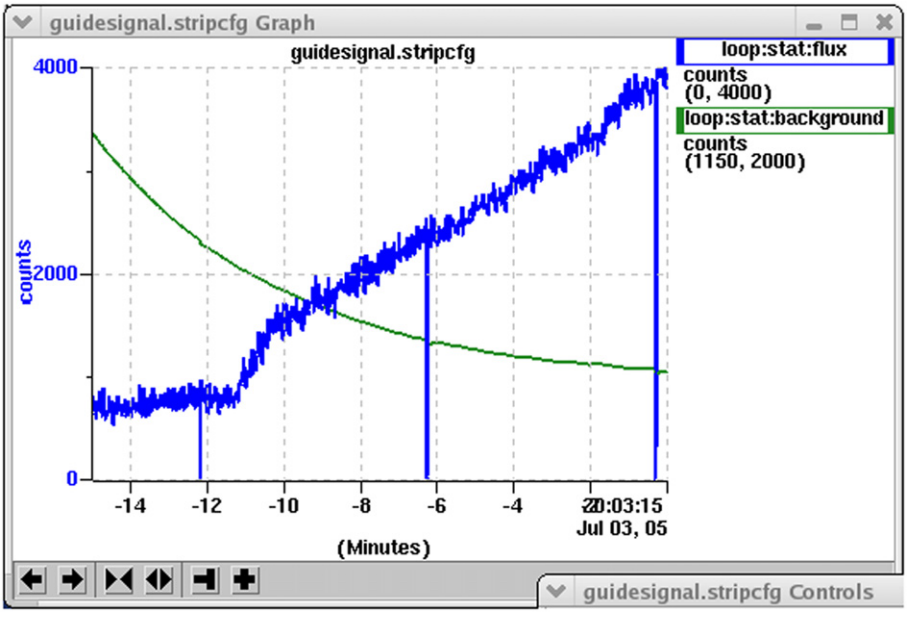

Fig. 1. The raw light curve produced by the UKIRT (red sensitive) guider camera on the night of July 3, 2005, Hawaii Standard Time (July 4 UT). The trace is timestamped at 20:03:15 HST by the telescope control system. The thick trace represents the brightness of the comet in the UKIRT $1.8'' \times 1.8''$ guider "box." The thin trace shows the brightness in the surrounding twelve $0.9'' \times 0.9''$ pixels, and represents the brightness of the sky. NB the apparent drop-out in guider counts every 6 min is due to the telescope beam switch.

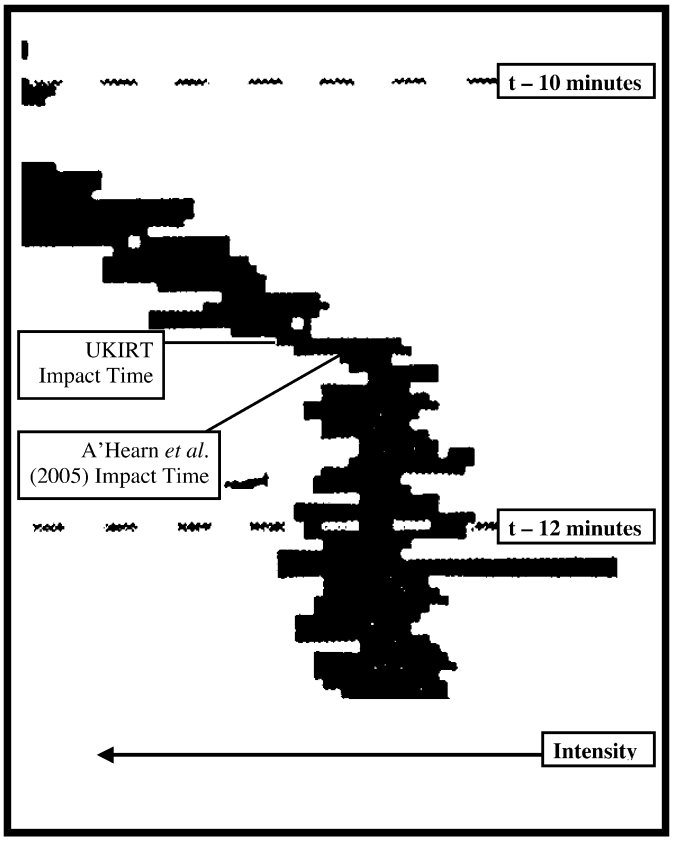

Fig. 2. Raw light curve around impact time, showing UKIRT determination of Impact Time. Impact Time derived by A'Hearn et al. (2005) is also shown.

ground-based observations recorded this flash. It is therefore probable that our light curve picks up the first evidence of material ejected as the crater is forming. This would be in the 1–10-s time frame outlined by Schultz et al. (2006), in which they describe a "diffuse plume of fine ejecta" expanding rapidly above the impact site.

Fig. 3a presents the light curve for 6 min immediately following impact in more detail, with the intensity scaled to the comet's pre-impact brightness (PIB). This curve, and others, have been produced by electronically digitising screen captures of the guider trace. A blow up of the two-minute period around impact, corresponding to between $t = -12$ and $t = -10$ min as shown in Fig. 1, is shown in Fig. 3b. After impact, there is a very rapid increase in intensity that peaks at $t = 7 \pm 1$ s, and then declines to reach a local minimum at $t = +12 \pm 1$ s. From then, the comet's brightness increases approximately linearly for the next 50 s until it reaches 1.94 PIB. Within six minutes of impact, the comet has brightened by a factor of 3.5. There are other possible structures, similar to our $t = 7$ s peak that are of similar, though somewhat lower, S/N, such as one around 30 s. Apart from indicating that the ejection was probably not a "smooth" process, we are not able to give further significance to these.

The full UKIRT light curve from impact time to 08:40 UT, when the comet set as far as UKIRT's ability to follow it was concerned, is shown in Fig. 4. The grey curve in this figure is the raw light curve, indicated by the guider trace. But this curve has

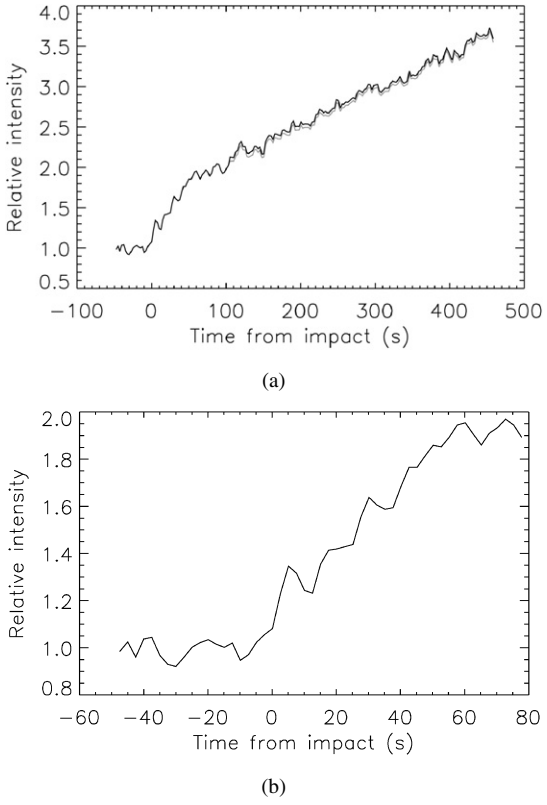

Fig. 3. (a) Initial increase in intensity up to 6 min post-impact. (b) Blow up of 2-min period around impact, showing the initial doubling in brightness of the comet.

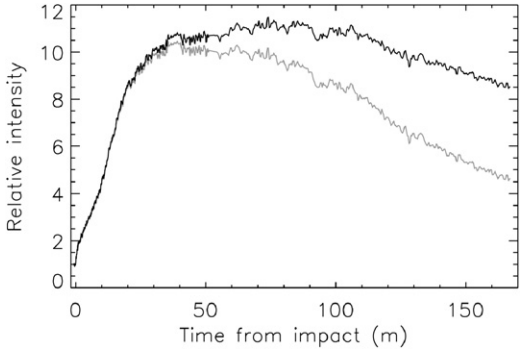

Fig. 4. UKIRT *R* light curve for the full night's observing on July 4, 2005 UT. The light trace shows the raw light curve. The dark trace includes correction for coma intensity in the twelve "sky" pixels.

to be corrected at later times for the fact that the comet's coma spreads into the twelve pixels that surround our target box. This causes the sky-subtraction process to overestimate the sky brightness, and make the comet appear less bright than it should be. The dark curve is the true light curve of the intensity at *R* of the comet and its coma, corrected for this "over-subtraction"; in doing that we assume that the "true" sky intensity is constant at the minimum value reached in the raw sky trace. As discussed by Meech et al. (2005), light curves from ground-based observatories show that the brightening has several phases. For our light curve, the initial, near-doubling in brightness over the first minute, is followed by a slower, nearly linear intensity increase until around $t = +10$ min. By this time, the comet is ~4 times

Table 1
Relative rates of brightening (RRB) for near-linear intensity increase regions

Time period post-UKIRT Impact Time (s)	RRB = $\Delta[I(t)/\text{PIB}]/\Delta t$ (units s^{-1})
12–62	1.3×10^{-2}
62–600	4.3×10^{-3}
600–1200	7.8×10^{-3}

brighter than pre-impact. During the next 10 min there is another near-linear increase, until the comet is 8.7 PIB. The time periods and relative rates of brightening (RRB), compared with the comet's pre-impact brightness, are given in Table 1. Note that $I(t)$ is dimensionless, since it is the actual brightness at time t divided by the brightness at Impact Time.

From $t = +20$ min onwards, the increase in brightness is falling off with time, such that the light curve has a domed appearance. At $t = +35$ min, the light curve is almost at maximum and there is a noticeable difference between the corrected and uncorrected light curves. This shows that cometary debris from the impact is passing out of the central four-pixel target box, into the surrounding pixels. The intensity measured in the target box now remains almost constant, peaking at ∼10.8 PIB, until $t = +110$ min, when it starts to decline approximately linearly until UKIRT is no longer able to follow the comet across the night sky, at $t = +170$ min. We interpret the UKIRT light curve as follows:

1. The very rapid intensity increase to the 05:52:12 UT, $t = +7$ s, peak represents the immediate ejection of "fine" material from the impact site, possibly still hot;
2. The following rapid intensity increase up $t = \sim 1$ min represents the ejection of rock and icy dust grains;
3. The slower increases in brightening up to $t = +35$ min indicates the icy dust and rock, excavated by the shock blast to form the impact crater, expanding such that new surfaces are exposed to sunlight. Further fragmentation of larger excavated rocks and grains is also probably occurring;
4. Reaching the intensity maximum at $t = \sim 35$ min, together with the commencement of the intensity increase in the "sky" intensity, indicates that the new coma material has completely filled the UKIRT target box and that the fastest fragments are beginning to pass into areas of the sky covered by the surrounding twelve pixels used for sky subtraction;
5. The onset of intensity decrease from the maximum around $t = +110$ min min indicates that even the material ejected at slower velocities is passing out of the target box.

These stages are in accordance with those discussed in Meech et al. (2005). If we accept reaching maximum intensity as indicating that our target box is completely filled, the expansion velocity of the new coma is 390 ± 20 m/s, slightly lower than the 450 m/s first announced by the UKIRT team (UKIRT team posting of 4 July, 2005, on DI Collaborator website: http://deepscience.astro.umd.edu/collab/summary/). This means that the expansion velocity now reported by the Hubble Space Telescope Team (Feldman et al., 2005) is in reasonably good agreement with our value. A more conservative calculation of the expansion velocity would be to use $t = +110$ min, when a clear decline in brightness is observed, to indicate the new coma material that is ejected at lower velocities passing out of our target box. This would give an expansion rate of 125 ± 20 m/s, and is probably a reasonable estimate of the average expansion rate of the ejecta material that is travelling at slower velocities. These values are close to, if slightly less than, the 400 and 150 m/s reported by Jehin et al. (2006) from the VLT and Keck observations for the gas and dust components, respectively. Our average velocity is 260 ± 15 m/s, somewhat faster than the 200 ± 20 m/s reported by Meech et al. (2005), based on imaging over the first 20 h post-impact.

Table 2
Seeing effects as a function of time post-UKIRT impact

Post-impact time (min)	Time to setting (min)	Airmass	Point spread function—FWHM (arcsec)	% of cometary brightness in surrounding pixels
+35	135	1.00	1.0	5
+50	120	1.20	1.1	8
+100	70	1.36	1.2	12
+120	50	1.55	1.3	18
+140	30	1.75	1.4	24
+170	Sets	2.00	1.5	31

Some caution is necessary in interpreting the R light curve after it reaches its maximum intensity, around $t = +35$ min, until it sets at $t = +170$ min. This is because the airmass of the comet—defined by $\sec(\theta)$, where θ is the zenith angle of the object being observed—is increasing. The effect of this is to increase the effective seeing, so that an increasing fraction of the light in the target box falls into the surrounding pixels. Table 1 shows this, in terms of the post-impact time and the comet's airmass, assuming that the seeing at $t = +35$ min was 1″.

Table 2 indicates that ∼26% of the decline in brightness of the comet from the peak intensity to its setting could be due to seeing effects, rather than material passing through the target box into the surrounding pixels. That does not affect our arguments concerning the maximum expansion velocity of 390 m/s. But, as the effects due to degraded seeing have increased by a factor of ∼3 around the time that the linear decrease in brightness commences, the slower expansion velocity of 125 m/s may need to be even lower. But by how much?

At $t = +110$ min, the time at which we designate for the true onset of decline from maximum brightness, Fig. 4 shows that the uncorrected light curve is 28% below the corrected curve. Table 2 shows that 15% of this may be accounted for by seeing effects, compared with just 5% at $t = +35$ min, around the time that maximum (corrected) brightness is reached. So the true light curve could actually still be increasing in brightness by as much as a further 7% above the maximum shown in Fig. 4. At $t = +170$ min, the corresponding values are 50 and 31%. But the corrected light curve is still only 22% below its peak value, leaving another 9% that could be added to the maximum value. So, comparing the $t = +110$ min and $t = +170$ min values, we can see that there is a possible additional 7% brightness above

maximum at $t = +110$ min and 9% at $t = +170$ min, which could indicate the comet was still brightening. That would make it impossible for us to determine the velocity of the slower moving ejecta from our observations, since they would not extend beyond the truly true onset of intensity decline.

It is difficult to quantify the effect of increasing effective seeing precisely, however, because it is well known that the seeing on Mauna Kea improves after sunset, as air conditions stabilise. That makes the values given in Table 2 maximum seeing effects. This tendency for seeing to improve after sunset would then offset the degradation of seeing due to increasing airmass. One more complicating factor would be a continued darkening of the sky, which would also lead to the slow component velocity being higher, although this is unlikely much later than 2 h after sunset. At this stage, therefore, we prefer to retain the low velocity value of 125 ± 20 m/s, recognising that it is probably an upper limit.

3. Water lines in Tempel 1

3.1. Background

The low temperatures associated with comets and the presence of water in the Earth's atmosphere are serious impediments to observing water lines in comets. The reason is that all the strong water lines emitted from the comas of comets are fundamental transitions, that is to say are due to transitions from a ro-vibrationally excited state to a ground vibrational state. Since these ground states are highly populated by water molecules at the low temperatures existing in the Earth's atmosphere, the incoming photons are absorbed. Nevertheless, despite these difficulties, it is essential to be able to quantify water emissions from comets, since water is the dominant ice in comets and, within 3–4 AU of the Sun, its sublimation controls the release of other volatiles.

Consequently, attention has focussed on other methods of measuring cometary water. In recent years, it has been realised that certain weaker transitions are not absorbed by the Earth's atmosphere. These are, solar-pumped non-resonant fluorescent (SPF) water lines. These lines originate in non-LTE regions of the comet's coma. They are transitions from higher-lying ro-vibrational states that have been 'pumped' by solar photons, down to intermediate ro-vibrational states. In LTE environments, where collisional de-excitation dominates, these upper levels would only be significantly populated at temperatures of several thousand Kelvin. However in non-LTE environments, such as exist in the coma of comets, they are able to remain populated for periods long enough to allow spontaneous radiative de-excitation.

Because they originate in non-LTE regions the intensities of SPF transitions are difficult to interpret. The methodology is detailed in Dello Russo et al. (2000) and relies on a knowledge of the upward and downward routes by which the upper state may become populated, the incident fluxes at the appropriate wavelengths and the relevant Einstein A and B coefficients. Most of this information is not available experimentally. But it is available in a high-accuracy calculated water linelist known as BT2 (Barber et al., 2006). SPF transitions have be used to determine the rotational temperatures and water-loss rates of comets (Dello Russo et al., 2004) and their primordial nuclear spin temperatures (Dello Russo et al., 2005; Kawakita et al., 2006).

3.2. Observations at 2.9 μm

Our principal objective in observing Tempel 1 was to determine the temporal development of SPF water lines following the Deep Impact event. We obtained spectra in the wavelength range centred on 2.894 μm, with a spectral range of ±0.040 μm. This wavelength region was selected because it was known to contain a number of SPF transitions (Dello Russo et al., 2004). It was also known to be an area of the spectrum which is largely void of other molecular species (such as CO) which means that it is possible to model this region using the BT2 synthetic water linelist (Barber et al., 2006), without having to include other species.

On the night prior to impact, when we were observing with UKIRT, water lines in Tempel 1 were not sufficiently bright for us to be able to obtain immediately useful data; this was also the case for the night immediately after impact, although work is continuing to analyse data from both nights. The results presented here, therefore, relate only to the period of 144 min immediately following impact during which we could still observe Tempel 1, before it set below the UKIRT horizon at 2 airmasses. Cometary spectra were produced using normal techniques for observing in the infrared *L* band. Flat field frames and standard star frames were obtained at the beginning an end of the observing session. For both the standard star and the comet, an individual spectrum was obtained with four co-added 10-s exposures, repeated four times in 2×2 sampling so that the effects of bad pixels were minimised. Each spectral frame thus corresponded to 160-s exposure. We operated in the normal ABBA mode. The telescope was first positioned such that light from the star or the comet fell onto Row 95 of the detector. After an initial observation, the A frame, the telescope was nodded 10″ so that light from the comet continued to fall on the spectrometer slit, but on a different row of the detector—Row 117. This produced a B frame.

A spectrum of the standard star ρ Virginis, used for flux calibration, is presented in Fig. 5 for our entire spectral region. This shows that the sky absorbed >95% of all extra-terrestrial emission in several parts of the spectrum. We thus decided to concentrate on the region from 2.8945 to 2.8985 μm, a region for which sky extinction is relatively low (unshaded portion of Fig. 5). Since the signal from the comet was from the spatially compact inner coma, we estimate that approximately 70% of the signal was contained within a single pixel row, and care was taken, when setting up the 'nod' parameters for the telescope beam-switching, to ensure that both the A and B signals were centred on pixel rows.

Comet Tempel 1 was observed using continuous ABBA quads, each quad being obtained over a period of 12 min; quads could later be summed or sampled as required. To produce our spectra and to investigate their temporal evolution, temporally

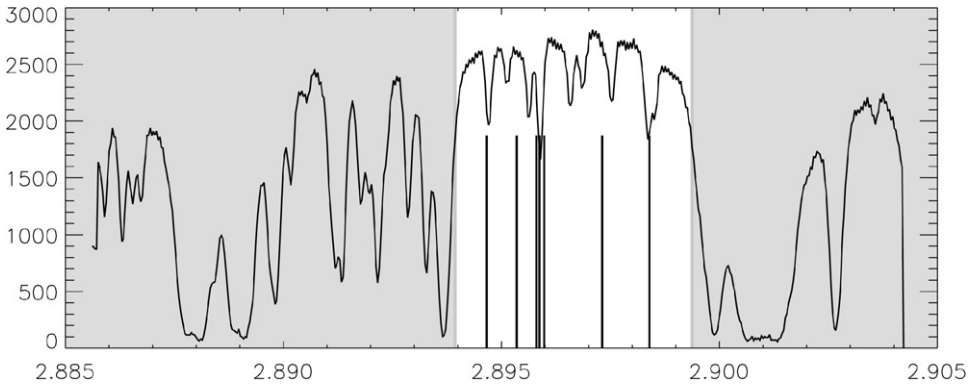

Fig. 5. Spectrum of ρ Virginis taken on July 4, 2005 UT, showing sky absorption in the full spectral region covered by the UKIRT CGS4 spectrometer. The unshaded region, for which sky absorption is consistently <50% of the maximum, is that used for the spectroscopic study presented here. NB the x-axis wavelength scale is in microns and the y-axis intensity scale is in arbitrary counts.

adjacent pairs of spectral frames were subtracted. This process has the effect of removing any dark current recorded on the detector, which is constant in time. The subtraction leaves an A–B frame, which has a positive spectrum of the comet in Row 95 and a negative spectrum in Row 117. There may also be some signal from the sky, which can vary from frame to frame. Finally, the spectrum in Row 117 was extracted and subtracted from that extracted from Row 95. This final process corrects for any sky variability, important in removing the effects of atmospheric water absorption. The net result is a spectrum that has an effective 320-s exposure, obtained (because of overheads such as nodding the telescope and reading out the detector array) over a period of ∼330 s. This, then, is the finest time resolution that the UKIRT Tempel 1 spectra can effectively sample. It should be noted that our analysis was confined to the signal in Rows 95 and 117; no attempt was made to extract the small amount of signal from adjacent rows as an analysis of the data revealed that this would have resulted in a reduction in the overall S/N ratio. UKIRT's guidance system tracks to high accuracy, and a subsequent analysis of the data revealed that there had been no detectable drift in the position of the signal on the array during the course of the evening.

In order to be able to identify water features, and to accurately measure their intensities, it was essential to compensate for the transmission of the Earth's atmosphere as a function of wavelength. This generally involves dividing the spectrum obtained after sky subtraction by a function that accurately represents the telluric transmission. In theory, we could have used the contemporary sky data, extracted from rows on the detector that did not have any cometary signal, to divide out the telluric transmission effects. However, in practice the low signal to noise obtained in an individual spectrum introduced a new element of noise into our data. In the end, we divided by the standard Keck sky transmission spectrum produced for the Deep Impact observations (Dello Russo, personal communication). This means that our derived intensities are directly comparable to those obtained by Keck on Impact Night (see below).

The detector was wavelength calibrated by matching observed sky lines with those in the Kitt Peak sky atlas downloadable from ftp://ftp.noao.edu/catalogs/atmospheric_transmission/ and also by comparing Keck sky data, which has the advantage of having a nearly identical water load to that at UKIRT. The two sets of reference data (Keck and Kitt Peak) were found to differ by up to 1.3×10^{-5} μm, equivalent to 0.36 of our pixel resolution of 3.62×10^{-5} μm. A second factor limiting the accuracy with which we were able to wavelength calibrate our observations was the non-linearity of the detector, which we estimated could deviate from linearity by one pixel over the 2.8945–2.8985 μm region. This meant that our estimated wavelength could be out by as much as 5×10^{-5} μm.

A detailed examination of the 24 A–B pairs revealed that sets 3, 4, 6, 11, 15 and 24 had excessively low S/N ratios and were therefore excluded. The post-impact total spectrum obtained by summing the other 18 A–B pairs, adjusted for a red shift of 9 km s^{-1}, is shown in Fig. 6 and covers the period 2005 July 4, 05:54 to 08:11 UT, but with 5 gaps each of ∼6-min duration starting at 6:06, 6:12, 6:24, 6:54 and 7:17 UT. The data have been adjusted to remove the continuum, which averages 3×10^{-16} W m^{-2} μm^{-1} across our spectral range. Negative intensities are due to noise, which we estimate to be in the region of $\pm 0.4 \times 10^{-16}$ W m^{-2} μm^{-1}. All of the features visible in Fig. 6 were present in the pre-processed spectrum: division by the Keck standard sky transmission spectrum did not produce previously unseen spectral features, but it did change the relative intensities of the features we report here. Some of the features in the spectrum have been labelled SPF or SH, and we now discuss the significance of these labels.

3.3. Solar Pumped Fluorescence (SPF) lines

Examination of Fig. 6 shows that two bright transitions at 2.8958 and 2.8983 μm stand out against a background of weaker features; the former has an intensity of 9.4×10^{-16} W m^{-2} μm^{-1}, the latter 3.9×10^{-16} W m^{-2} μm^{-1}. These features are at wavelengths where solar pumped fluorescence (SPF) lines have previously been identified (Dello Russo et al., 2004, 2005); their intensities, relative to other features we discuss in the following section are enhanced by a factor of ∼4 by the process of dividing by the Keck standard spectrum, described above.

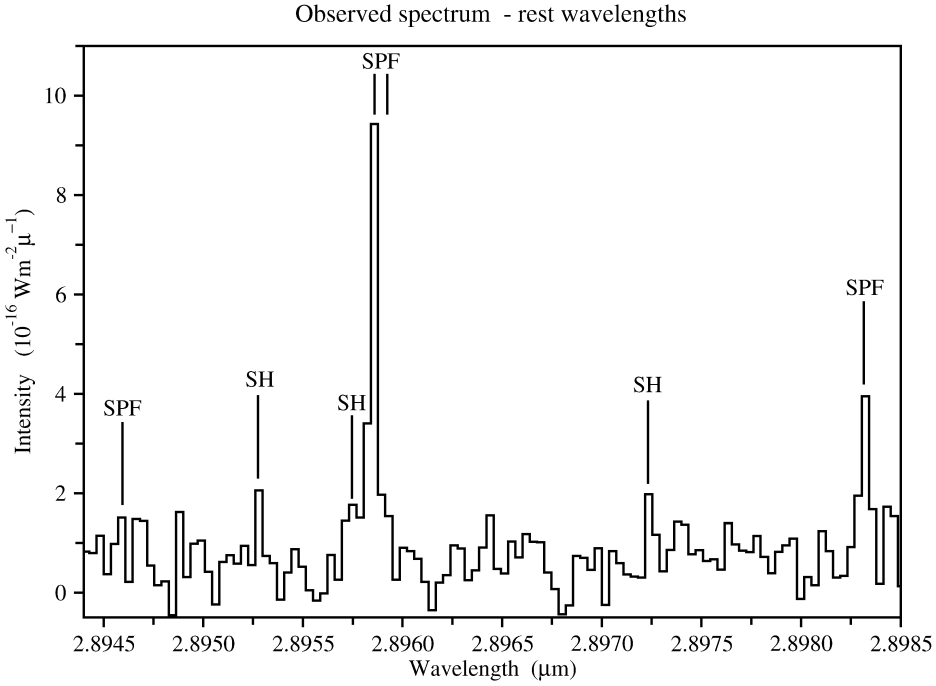

Fig. 6. Full night spectrum from 2.894 to 2.899 μm used in this study. Features are labelled according to Table 3, where the line assignments are also given.

Table 3
Observed water lines, identifications and excitation mechanisms

λ (observed) (μm) (±0.00005)	Identification (see text for notation)	λ (laboratory) (μm)	A_{if} (calculated) (s^{-1})	Type
2.89458	(101)[211]–(001)[220]	2.89462	1.9	SPF
2.89527	(103)[110]–(102)[110]	2.89526	53.5	SH
2.89527	(211)[322]–(210)[211]	2.89528	8.5	SH
2.89573	(210)[101]–(011)[000]	2.89570	5.1	SH
2.89580	(200)[110]–(100)[221]	2.89578	4.7	SPF
2.89591	(101)[202]–(100)[321]	2.89590	1.7	SPF
2.89723	(220)[212]–(021)[111]	2.89728	4.4	SH
2.89831	(200)[110]–(001)[111]	2.89830	6.6	SPF

Water lines are assigned the normal vibrational and rotational quantum numbers for the purpose of identification: (v_1 v_2 v_3) refer to the number of quanta in the H_2O symmetric stretch, v_1, the bending mode, v_2, and the asymmetric stretch, v_3, respectively, and the labels [J K_A K_C] refer to the total angular momentum, and its projection on the molecular A and C axes, respectively. The strongest feature in Fig. 6 at 2.8958 μm is a blend of (200)[110]–(100)[221] at 2.89578 μm and (101)[202]–(100)[321] at 2.89590 μm (see Table 3). The weaker feature at 2.8983 μm is (200)[110]–(001)[111]. Within our spectral range there is also a very weak SPF feature at 2.89458 μm due to (101)[211]–(001)[220], which is barely distinguishable in our spectrum.

Explaining the intensities of SPF lines, and deriving physical parameters such as water abundances and production rates, requires detailed modelling that is beyond the scope of this paper (see Dello Russo et al., 2004, 2005). Instead, we compare our intensities with those obtained during Impact Night on the Keck Telescope by Mumma et al. (2005). The easiest comparison feature is that at 2.8958 μm, which corresponds to 3453.3 cm^{-1}. The Keck intensity in this feature is $\sim 1.2 \times 10^{-18}$ W m^{-2} [cm^{-1}]$^{-1}$, which corresponds to an intensity of 1.7×10^{-19} W m^{-2} integrated across the line. The UKIRT integrated intensity is 1.5×10^{-19} W m^{-2}, in good agreement with Mumma et al.'s (2005) figure, given that the observing periods at Keck and UKIRT do not precisely correspond (see below for further discussion of this). Post-impact on 2005 July 4 UT, the Keck values of water abundance, $N(H_2O)$, ranged from $859 \pm 97 \times 10^{28}$ to $1192 \pm 227 \times 10^{28}$ in the beam, dependent on time and wavelength range, and the water production rate, $Q(H_2O) = 1703 \pm 192 \times 10^{25}$ to $2100 \pm 400 \times 10^{25}$ s^{-1}. The mean values (over four reported sets of observations) are $N(H_2O) = 1020 \pm 60 \times 10^{28}$ and $Q(H_2O) = 1840 \pm 110 \times 10^{25}$ s^{-1}. Pre-impact on 2005 July 4, the corresponding values were $558 \pm 99 \times 10^{28}$ and $1037 \pm 174 \times 10^{25}$ s^{-1}. These figures show that the impact resulted in a ~75% increase in $Q(H_2O)$ and a ~80% increase in the column abundance. While we cannot independently model these results, it is clear that our post-impact spectrum gives further support to Mumma et al.'s (2005) figures.

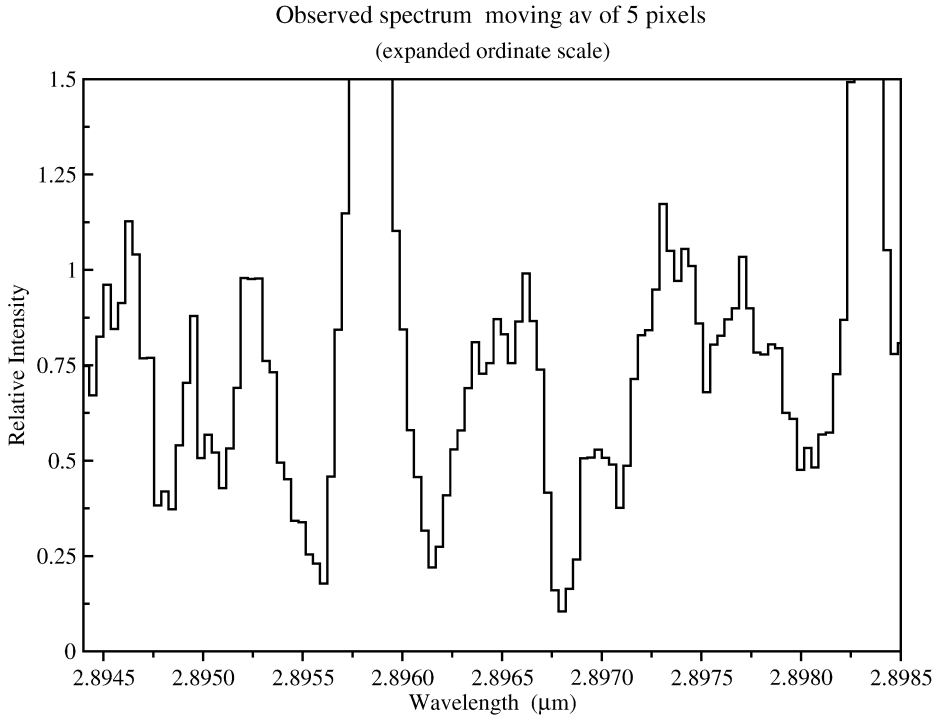

Fig. 7. Low intensity component of the full night spectrum, with the spectral resolution degraded to $\lambda/\Delta\lambda = 3700$. The intensity units are now arbitrary, following the broadening process.

3.4. Weaker spectral features

In addition to the SPF transitions identified in Fig. 6, there are also a number of weaker spectral features where the S/N ratio is greater than 4 and which, unlike noise, appear in the same place (albeit with differing intensities) in many of the individual frames. Many of these have been labelled SH, which we now explain with reference to the BT2 linelist. In order to do this we have to take account of the fact that there are inaccuracies both in the wavelength calibration of our detector, estimated to be in the region of 5×10^{-5} μm (see earlier), and in the frequencies of the BT2 linelist, some of which are up to 5×10^{-4} μm. To identify the weaker lines, we therefore reduce the resolution of our observed data from 18,500 to 3700 by taking a boxcar average of five pixels. Fig. 7 shows the resulting observed spectrum. In this figure the vertical scale is terminated at a level below the peak intensities of the two strongest SPF transitions, to enhance the visibility of the weaker features.

Fig. 8 shows a series of synthetic spectra derived from the BT2 linelist (with some corrections to the calculated wavelengths based on experimental data, where available). These spectra, which assume LTE) were generated at 3000, 4000 and 5000 K. We also applied the restriction that only states with $J \leqslant 3$ are included, but placed no restriction on vibrational quantum numbers. The resolution in Fig. 8 was set to be the same as Fig. 7. Fig. 8 is therefore a "high-v, low-J" spectrum and it is observed that it reproduces the line positions well, of many of the non-SPF features in the low resolution observed spectrum, Fig. 7. It should be noted that similar features are observed in synthetic spectra generated for temperatures greater than 3000 K and the appearances of the spectra vary little once $T_{\mathrm{vib}} > 4500$ K, except for increasing in overall intensity. Fig. 9 shows another set of synthetic BT2 spectra generated at the same three temperatures, but this time including all J levels (up to 50). Many of the same features are observed as in Fig. 8. The relative intensities of the SH features will depend on the exact mechanism by which the upper levels are populated. Here we have assumed LTE, for want of anything more sophisticated, and it is clear that the observed relative intensities of the SH features (Fig. 7) are only approximately reproduced in the modelled spectra (Figs. 8 and 9). A complicating factor may also be that the continuum has some wavelength dependence that cannot be independently assessed, in the absence of detailed modelling.

Although the features produced from the BT2 linelist in Figs. 8 and 9 are blends of several transitions, it is possible to identify certain dominant transitions. Thus our spectrum includes several transitions from states that include one or more quanta of ν_2, or that involve 4 vibrational quanta overall, that are not normally observed as part of the suite of SPF spectral features. These include a blend of (103)–(102) and (211)–(210) at 2.8953 μm, and (220)–(021) at 2.8972 μm. We consider the upper levels with more than two quanta to have been populated by a—secondary in importance—mechanism, different from that which populates the (200) or (101) levels: whereas the SPF transitions originate from upper states having energies in the region of 7300 cm^{-1}, the transitions that we have labelled SH all originate from higher energy states (those upper states having four vibrational quanta are in the energy range 10,300–14,400 cm^{-1}). Table 3 gives our overall identifications of the spectral features observed from UKIRT that we have been able to identify.

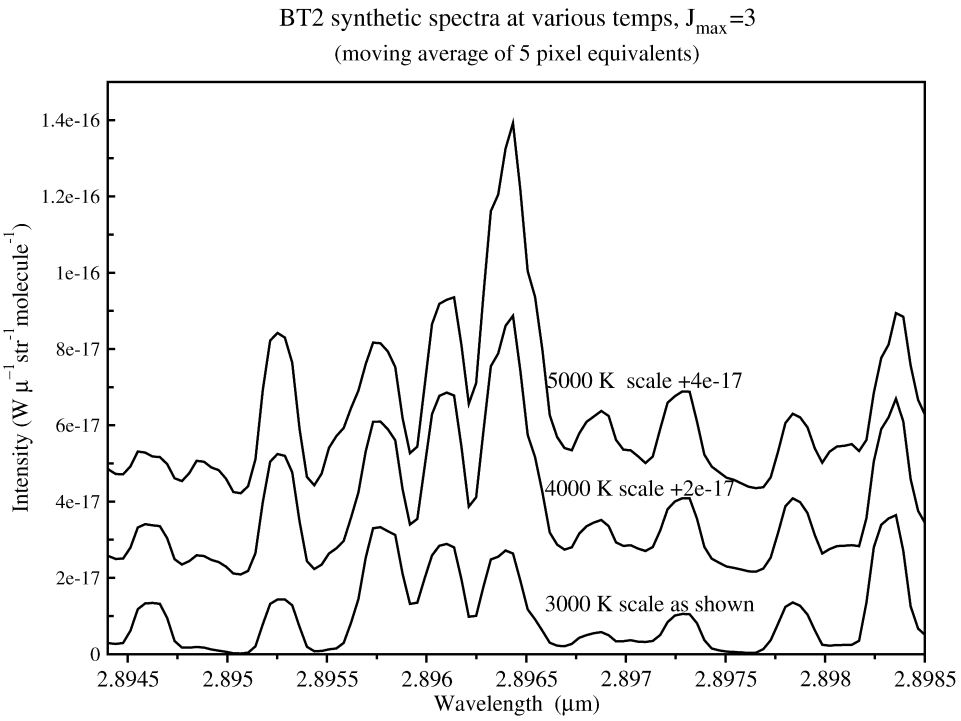

Fig. 8. Simulated hot water spectrum from 2.894 to 2.899 μm at a resolution of $\lambda/\Delta\lambda = 3700$. The spectrum makes use of the BT2 linelist, restricted so that only transitions up from $3 \geqslant J$ are used.

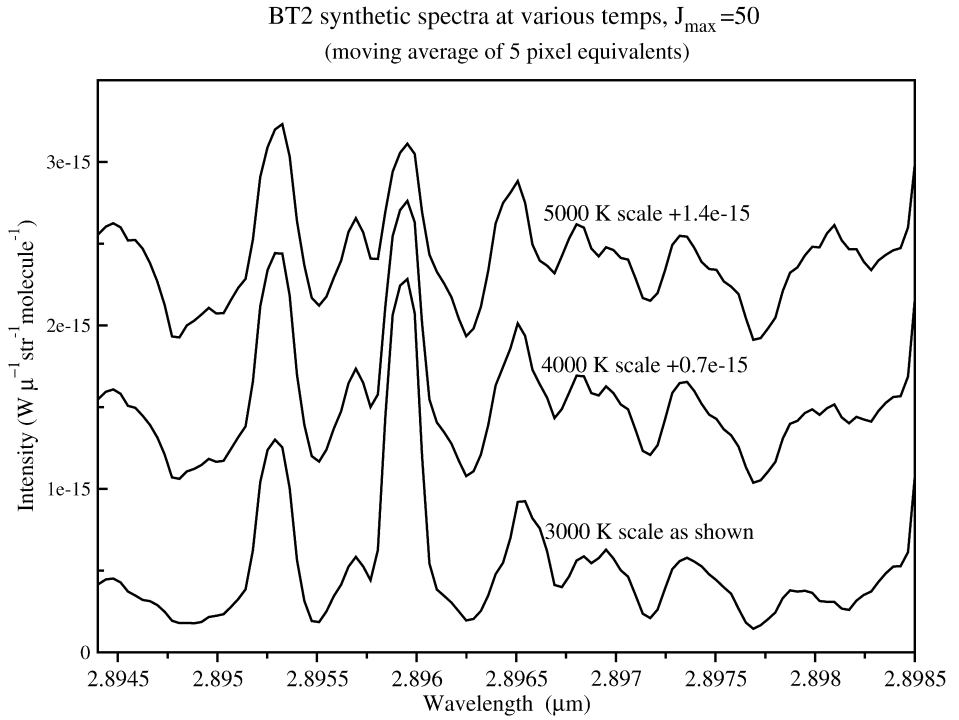

Fig. 9. Simulated hot water spectrum from 2.894 to 2.899 μm at a resolution of $\lambda/\Delta\lambda = 3700$. The spectrum makes use of the full BT2 linelist.

It is possible that the spectral features that we label SH are in some way related to water molecules that, under the action of sunlight, have sublimed from freshly exposed icy grains resulting from the impact. Spectra in the interstellar medium with high-v, low-J characteristics—corresponding to Fig. 8—are produced by a mechanism known as stochastic heating (Draine and Saltpeter, 1979; Evans, 1994; Creigham et al., 2006).

As far as the positions and intensities of the observed SPF transitions are concerned, our results agree well with those of Mumma et al. (2005). However, none of the SH features that we

identify appear in Mumma et al.'s spectrum. One possible reason for the difference between our results and those of Mumma et al. is the difference in times during which the spectra were obtained. Our results were obtained between 05:54 and 08:11 UT. on impact night, whilst Mumma et al.'s spectrum was obtained between 6:43 and 7:25 UT. Although we do not present the temporal behaviour of our spectra in this paper, a frame-by-frame examination of our data shows that the SH features were stronger during the first ∼50 min after impact and then decreased in intensity. This means that if our observations are correct, Mumma et al.'s spectra at this wavelength were obtained after the SH lines had already weakened.

4. Conclusions

The Deep Impact collision with Comet 9P/Tempel 1 clearly succeeded in releasing considerable amounts of fresh material from beneath the immediate surface, although—as others have commented (e.g., Mumma et al., 2005)—this body seems to have had less volatiles than other comets. The *R* light curve shows a number of distinct phases from immediate heating through to a major expansion of the sunlight-reflecting coma. It would also be interesting to investigate the temporal evolution of the observed water lines. This will take a considerable amount of data processing, however, since the individual spectral pairs produce rather noisy spectra. We have not addressed this issue here, therefore, and have confined our comments to spectral data integrated over the whole of the observing period. This has enabled us to identify water lines in the post-impact spectrum of Comet Tempel 1 that have not previously been recorded in cometary spectra. These are the SH lines in Fig. 6 and Table 3, but our designation should not be interpreted as implying that we fully understand the mechanism by which they are formed. Recently we have obtained UKIRT spectra of Comet 73P Fragment C, to investigate whether this fragmented and fragmenting comet has similar SH features to Temple 1. Work is continuing.

Acknowledgments

We acknowledge the considerable assistance afforded to us by Mike Mumma, in discussions prior to impact, which helped us prepare our observations, and after impact, in sending us an advanced copy of his 2005 paper. Neil Dello Russo is also thanked for his very helpful input throughout this period. UCL colleagues Serena Viti and Jeremy Yates are thanked for their advice on the relevance of stochastic heating in the ISM. The UK Particle Physics and Astronomy Research Council, which funds UKIRT, are thanked for fellowships to R.J.B. and T.S. This paper has been significantly improved by the helpful comments of our two referees, to whom many thanks are also due.

References

A'Hearn, M.F., and 32 colleagues, 2005. Deep Impact: Excavating Comet Tempel 1. Science 310, 258–264.

Barber, R.J., Tennyson, J., Harris, G.J., Tolchenov, R.N., 2006. A high accuracy computed water linelist. Mon. Not. R. Astron. Soc. 368, 1087–1094.

Creigham, S.C., Perry, J.S.A., Price, S.D., 2006. The rovibrational distribution of H_2 and HD formed on a graphite surface at 15–50 K. J. Chem. Phys. 124, 114701.

Dello Russo, N., Mumma, M.J., DiSanti, M.A., Magee-Sauer, K., Novak, R., Rettig, T.W., 2000. Water production and release in Comet C/1995 O1 Hale–Bopp. Icarus 143, 324–337.

Dello Russo, N., DiSanti, M.A., Magee-Sauer, K., Gibb, E.L., Mumma, M.J., Barber, R.J., Tennyson, J., 2004. Water production and release in Comet 153P/Ikeya–Zhang (C/2002 C1): Accurate rotational temperature retrievals from hot-bands near 2.9 μm. Icarus 168, 186–200.

Dello Russo, N., Bonev, B.P., DiSanti, M.A., Mumma, M.J., Gibb, E.L., Magee-Sauer, K., Barber, R.J., Tennyson, J., 2005. Water production rates, rotational temperatures, and spin temperatures in Comets C/1999 H1 (Lee), C/1999 S4, and C/2001 A2. Astrophys. J. 621, 537–544.

Draine, B.T., Saltpeter, E.E., 1979. On the physics of dust grains in hot gas. Astrophys. J. 231, 77.

Evans, A., 1994. The Dusty Universe. Praxis Publishing, Winchester, pp. 76–78.

Feldman, P.D., Weaver, H.A., A'Hearn, M.F., Belton, M.J.S., Meech, K.J., 2005. Hubble Space Telescope observations of Comet 9P/Tempel 1. Bull. Am. Astron. Soc. 37 (3). 42.04.

Jehin, E., Manfroid, J., Hutsemékers, D., Cochran, A.L., Arpigny, C., Jackson, W.M., Rauer, H., Schulz, R., Zucconi, J.-M., 2006. Deep Impact: High-resolution optical spectroscopy with the ESO VLT and the Keck I Telescope. Astrophys. J. 641, L145–L148.

Kawakita, H., Dello Russo, N., Furusho, R., Fuse, T., Watanabe, J.I., Boice, D.C., Sadakane, K., Arimoto, N., Ohkubo, M., Ohnishi, T., 2006. Ortho-para ratios of water and ammonia in Comet C/2001 Q4 (Neat): Comparisons of nuclear spin temperatures of water, ammonia and methane. Astrophys. J. 643, 1337–1344.

Meech, K.J., and 208 colleagues, 2005. Deep Impact: Observations from a wordwide Earth-based campaign. Science 310, 265–269.

Mumma, M.J., and 13 colleagues, 2005. Parent volatiles in Comet 9P/Tempel 1: Before and after impact. Science 310, 270–274.

Schultz, P.H., Ernst, C., A'Hearn, M.F., Eberhardy, C., Sunshine, J.M., and the DI Team, 2006. The Deep Impact collision: A large-scale oblique impact experiment. Lunar Planet. Sci. 37. Abstract 229.